Crystal Structures of Recombinant Human Dihydrofolate Reductase Complexed with Folate and 5-Deazafolate†

Jay F. Davies, II,‡,§ Tavner J. Delcamp,‖ Neal J. Prendergast,‖ Victor A. Ashford,⊥ James H. Freisheim,‖ and Joseph Kraut*,§

Departments of Chemistry and Biology, University of California, San Diego, La Jolla, California 92093, and Department of Biochemistry, Medical College of Ohio, Toledo, Ohio 43699

Received April 6, 1990; Revised Manuscript Received July 12, 1990

ABSTRACT: The 2.3-Å crystal structure of recombinant human dihydrofolate reductase (EC 1.5.1.3, DHFR) has been solved as a binary complex with folate (a poor substrate at neutral pH) and also as a binary complex with an inhibitor, 5-deazafolate. The inhibitor appears to be protonated at N8 on binding, whereas folate is not. Rotation of the peptide plane joining I7 and V8 from its position in the folate complex permits hydrogen bonding of 5-deazafolate's protonated N8 to the backbone carbonyl of I7, thus contributing to the enzyme's greater affinity for 5-deazafolate than for folate. In this respect it is likely that bound 5-deazafolate furnishes a model for 7,8-dihydrofolate binding and, in addition, resembles the transition state for folate reduction. A hypothetical transition-state model for folate reduction, generated by superposition of the DHFR binary complexes human·5-deazafolate and chicken liver·NADPH, reveals a 1-Å overlap of the binding sites for folate's pteridine ring and the dihydronicotinamide ring of NADPH. It is proposed that this binding-site overlap accelerates the reduction of both folate and 7,8-dihydrofolate by simultaneously binding substrate and cofactor with a sub van der Waals separation that is optimal for hydride transfer.

Dihydrofolate reductase (5,6,7,8-tetrahydrofolate:$NADP^+$ oxidoreductase, EC 1.5.1.3, DHFR[1]) catalyzes the NADPH-linked reduction of 7,8-dihydrofolate to 5,6,7,8-tetrahydrofolate. The enzyme is also capable of catalyzing the NADPH-linked reduction of folate to 7,8-dihydrofolate, but at a lesser rate, which varies among species. Interest in DHFR stems from its importance in several clinical areas. The participation of 5,10-methylenetetrahydrofolate in thymidylate synthesis couples the enzyme to cell division; consequently, DHFR is a target for antineoplastics such as methotrexate. Moreover, species-dependent differences in the enzyme's sensitivity to inhibitors are responsible for the efficacy of the antibacterial trimethoprim and the antimalarial pyrimethamine.

DHFR is a small, stable, and crystallographically well-behaved enzyme. It is therefore well-suited to high-resolution crystallographic studies. Because of these properties, this enzyme has been the subject of many structural, kinetic, and mutagenic studies. For reviews of these investigations, see Freisheim and Matthews (1984), Blakley (1984), and Kraut and Matthews (1987). Structures of a variety of substrate, cofactor, and inhibitor complexes, both binary and ternary, are now known for DHFR from *Escherichia coli* (Bolin et al., 1982; Filman et al., 1982), *Lactobacillus casei* (Bolin et al., 1982; Filman et al., 1982), chicken liver (Matthews et al., 1985a,b), L1210 mouse lymphoma (Stammers et al., 1987), recombinant human (Oefner et al., 1988), and type II resistant plasmid R67 of *E. coli* (Matthews et al., 1986). Recently, the gene encoding human DHFR was cloned and the enzyme expressed in *E. coli* as an aid to the extension of these investigations to the human enzyme (Prendergast et al., 1988). We report here the refined 2.3-Å crystal structure of human DHFR, both in binary complex with folate and as a binary complex with the potent inhibitor 5-deazafolate. The coordinates of these structures have been deposited with the Brookhaven National Laboratories Protein Data Bank and were assigned the following identification codes: the rhDHFR·folate complex is designated 1DHF and the rhDHFR·5-deazafolate complex as 2DHF.

Until recently, most kinetic studies have focused on the catalysis of 7,8-dihydrofolate reduction by DHFR. However, the susceptibility of 7,8-dihydrofolate and 5,6,7,8-tetrahydrofolate to oxidative degradation (Blakley, 1969) poses a serious obstacle to crystallographic studies of those ligands complexed with DHFR. As folate is relatively stable, it represents the most accessible means of gathering structural information on protein–substrate interactions to illuminate those factors responsible for catalytic rate enhancement of substrate reduction by NADPH.

Additional information on enzymic catalysis can be gleaned from studies on DHFR·inhibitor complexes. As measured by inhibition constants, 5-deazafolate binds more tightly than folate to *E. coli* (116-fold) and chicken liver (34-fold) DHFR (Stone et al., 1984). A basic tenet of transition-state theory holds that enzymic catalysis results from tighter binding of the transition state than of either substrates or products. Minor structural changes in a ligand that result in tighter binding, as is the case with 5-deazafolate, can provide insight into both the nature of the transition state and the enzyme–substrate

† This work was supported by NIH Training Grant T32 CA09523, NIH Grant CA 41461 to J.H.F., NIH Grant RR01644, a grant from the Markey Charitable Foundation, and NIH Grants GM10928 and CA17374 to J.K.

* Author to whom correspondence should be addressed.

‡ Present address: Agouron Pharmaceuticals, 11025 N. Torrey Pines Rd., La Jolla, CA 92037.

§ Department of Chemistry, University of California, San Diego.

‖ Medical College of Ohio.

⊥ Department of Biology, University of California, San Diego.

[1] Abbreviations: DHFR, dihydrofolate reductase; rhDHFR, rh, recombinant human DHFR; clDHFR, cl, chicken liver DHFR; ecDHFR, ec, *E. coli* DHFR; lcDHFR, lc, *L. casei* DHFR; $NADP(^+/H)$, nicotinamide adenine dinucleotide phosphate (oxidized/reduced); pABA, *p*-aminobenzoic acid; pABG, (*p*-aminobenzoyl)-L-glutamate; F_o, observed structure factor; F_c, calculated structure factor.

0006-2960/90/0429-9467$02.50/0

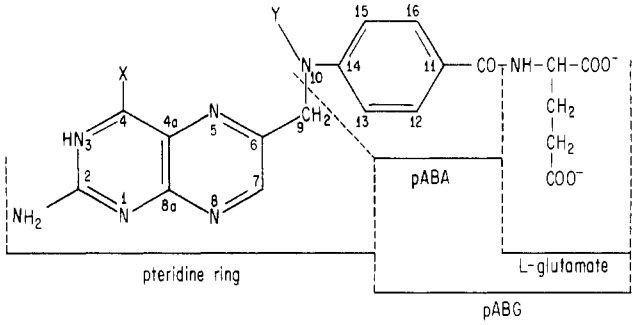

FIGURE 1: Covalent structure and atom numbering for folate (X = O4 and Y = H) or methotrexate (X = NH_2 and Y = CH_3).

interactions that serve to stabilize it.

METHODS

Folate Binary Complex of rhDHFR

Crystallization and X-ray Data Collection. Recombinant human dihydrofolate reductase was isolated from *E. coli* and purified as described elsewhere (Prendergast et al., 1988). The enzyme, in 0.05 M potassium phosphate and 1 mM dithioerythritol at pH 7.5, was concentrated to approximately 10 mg mL^{-1} by centrifugal ultrafiltration at 4 °C (Centricon-10, Amicon). A 0.05 M solution of sodium folate was prepared by dissolving folic acid (Sigma Chemical) in distilled water and adjusting the pH to 7.5 with sodium hydroxide. Dissolved folate was added to the protein until the final solution contained a 3-fold molar excess of substrate to enzyme. Five-microliter aliquots were then mixed with an equal volume of crystallization medium containing 0.30 M sodium acetate and 35% (w/v) poly(ethylene glycol) of molecular weight 4000 (PEG-4000, Sigma Chemical) adjusted to pH 5.9 (ambient temperature). The mixed solutions were suspended from silicone-coated cover slips as hanging drops over 1-mL reservoirs containing 0.17 M sodium acetate, 20% (w/v) PEG-4000, and 7% (v/v) ethanol. All crystals were grown at 4 °C. Yellow crystals in the shape of rods or square plates (0.6 × 0.6 × 0.2 mm) grew within several weeks. Crystallization was relatively insensitive to precipitant concentrations but did not occur with ethanol or PEG-4000 alone, or above pH 6.5. The crystals belong to space group $P1$ with unit cell dimensions a = 36.1 Å, b = 38.7 Å, c = 76.9 Å, α = 94.3°, β = 91.7°, and γ = 111.0°. The unit cell contains two rhDHFR molecules.

Prior to mounting in glass capillaries, crystals suitable for X-ray data collection were rinsed in reservoir solution to remove residual protein and phosphate buffer. X-ray diffraction data from two crystals were collected at ambient temperature (~20 °C) by using the UCSD multiwire area detector (Cork et al., 1973; Xuong et al., 1985). The two data sets were reduced independently to R_{sym} values of 0.036 and 0.034 based on an average of two observations per unique reflection.[2] Merging of these independent data sets was accomplished with the BOSS programs. The merging residual for 4216 pairs of common reflections was 0.056. The final data set of 16 023 unique structure factors was 91% complete to a Bragg spacing of 2.3 Å.

Molecular Replacement. A locally implemented version (Bystroff, 1988) of Crowther's fast rotation function (1972), as modified by Tanaka (1977), was used for molecular replacement. A self-rotation with the observed data revealed two solutions, indicating the presence of two molecules per unit cell related by an approximate 180° rotation. With the backbone and C_β coordinates of the refined 1.7-Å clDHFR·NADPH structure as a search model (S. J. Oatley, unpublished results), using a 10–4-Å shell of data and a 24-Å radius of integration, the rotation calculation yielded two solutions. With a model of rhDHFR constructed from the refined 1.7-Å clDHFR·NADPH structure and the known clDHFR – rhDHFR sequence differences (Kraut & Matthews, 1987), the vector relating these two orientations was determined by a translational R factor[3] search calculated with a locally developed program (Bystroff, 1988). The search, against a 5–7-Å data shell, was performed by fixing one molecule's center of mass at the unit cell origin while translating the second molecule first on a 1-Å grid for an approximate location and then on a 0.2-Å grid for greater accuracy. The R factor at the search minimum was 0.44, significantly below the 0.52 global average.

Crystallographic Refinement. Ten cycles of CORELS rigid-body refinement (Sussman et al., 1977) against the 70–9-Å shell of data resulted in an R factor of 0.32. As there are no symmetry operations to fix the translation of the molecules relative to the origin in space group $P1$, one molecule was held fixed during each cycle, with refinement alternating between molecule 1 and molecule 2. Further refinement was accomplished by utilizing the X-PLOR simulated annealing refinement package (Brünger, 1988b), as implemented on the San Diego Supercomputer Center (SDSC) Cray X-MP/48. Simulated annealing refinement has been demonstrated to yield a larger radius of convergence than conventional least-squares refinement (Brünger et al., 1987; Brünger, 1988a), thereby reducing the frequency of manual intervention in the refinement process. By use of X-PLOR, the model was subjected to 200 cycles of least-squares positional refinement, two cycles of molecular dynamics refinement (0.50 ps at 2000 K followed by 0.25 ps at 300 K), 60 cycles of positional refinement, and 20 cycles of atomic B-factor refinement followed by an additional 40 cycles of positional refinement. This process decreased the R factor from 0.456 to 0.255 for all data measured in the 15–2.4-Å shell.

At this point folate was fitted to the $F_o - F_c$ difference density at each catalytic site by using a Silicon Graphics IRIS 2400 work station running the molecular modeling programs FRODO (Jones, 1978), and MMS (Dempsey, 1987). The resulting model was then subjected to further least-squares refinement by using the program PROLSQ (Konnert, 1976; Hendrickson, 1981), as optimized for execution on the SDSC Cray X-MP/48 (Stuart Oatley and Susan Oatley, unpublished results). During refinement, a nonlinear F_c correction was applied to allow for the contribution of amorphous solvent to the X-ray scattering (Bolin et al., 1982). The final optimum values of the parameters uk and ub were 0.75 and 175, respectively. An additional F_c correction was applied to allow for the overall thermal anisotropy displayed by these crystals. Incorporation of this procedure into our version of PROLSQ has been described elsewhere (Wang, 1988; Wang et al., 1990). At various times during refinement portions of the model exhibiting ambiguous electron density in $F_o - F_c$ or $2F_o - F_c$ maps were deleted, the remainder of the model refined to convergence and the maps were recalculated. Atoms that failed to display interpretable electron density were omitted

[2] $R_{sym} = \sum_{hkl}(\sum_i|I_i - \bar{I}|/\sum_i I_i)$, where I_i is the ith observation of reflection I or a symmetry-related reflection and $\bar{I}$ the scaled mean intensity. The summation is over all measured reflections (hkl).

[3] $R = \sum_{hkl}|F_o - F_c|/\sum_{hkl}F_o$. The summation is over all measured reflections (hkl).

from the model. Water molecules assigned positions were those that represented peaks greater than 3σ in difference maps, were within 2.4–3.2 Å of a heteroatom, and possessed reasonable hydrogen-bonding geometry.

A total of 129 cycles of refinement were performed, resulting in a crystallographic R factor of 0.176 for all measured data to 2.3 Å, an rms deviation of bond lengths from their dictionary values of 0.020 Å, and an rms deviation of atoms from their least-squares plane of 0.015 Å. Atoms subject to planar restraint included the pteridine and pABA of folate, peptide planes, and aromatic side chains. These statistics correspond to a mean uncertainty in atomic position of 0.25 Å, as estimated by the method of Luzzati (1952). The numbering scheme for the two molecules in the unit cell is as follows: for molecule 1 the protein residues are numbered 1–186 and the bound ligand is 187; for molecule 2 the protein residues are numbered 201–386 and the bound ligand is 387; ordered solvent molecules are numbered sequentially from 401. The conformation of the three amino-terminal residues and the carboxy-terminal residue could not be determined unequivocally in either molecule 1 or 2 and they have therefore been omitted. Although N-terminal analysis indicates that 40% of the protein retains the initiator methionine (Prendergast et al., 1988), it was not seen in any maps. There also remains unmodeled density at the catalytic sites of molecules 1 and 2, despite repeated attempts to interpret it. In molecule 1 this density is in direct contact with N5 of folate and extends nearly parallel to the pABA moiety toward bulk solvent. The unmodeled density at the catalytic site of molecule 2 occupies a similar position but is less pronounced. The final structure (two molecules, 182 residues each) contains 2952 protein atoms, two folate molecules (64 atoms), and 116 ordered water molecules.

5-Deazafolate Binary Complex of rhDHFR

Crystallization and Data Collection. Synthesis of the inhibitor 5-deazafolate, a generous gift of John Montgomery, has been described elsewhere (Temple et al., 1982). Crystals of the rhDHFR·5-deazafolate binary complex were grown under conditions similar to those used to crystallize the folate complex except that the inhibitor was added to the protein solution as a solid before addition of crystallization medium. The crystals were isomorphous with those of the folate complex, with unit cell dimensions a = 36.1 Å, b = 38.5 Å, c = 76.8 Å, α = 93.9°, β = 91.4°, and γ = 111.5°. X-ray diffraction data were collected from one crystal at ambient temperature by using the UCSD multiwire area detector (Cork et al., 1973; Xuong et al., 1985). Data reduction yielded an R_{sym} value of 0.050 for a data set containing 15 545 unique structure factors that is 95% complete to a Bragg spacing of 2.3 Å.

Crystallographic Refinement. As a difference Fourier between the folate and 5-deazafolate complexes indicated no major rearrangements requiring manual adjustment, PROLSQ least-squares refinement was initiated by using the partially refined folate structure (PROLSQ cycle 42) as a starting model. To reduce bias, the inhibitor was deleted after 15 cycles of refinement and the remainder of the model was refined to convergence. Two 5-deazafolate molecules, one for each of the two enzyme molecules in the unit cell, were fitted to the resulting difference density in an $F_o - F_c$ omit map, and refinement continued as described for the folate complex. Water molecules were assigned independently in the folate complex and 5-deazafolate complex structures and, in the final models, waters deemed structurally equivalent in the two complexes (i.e., those within 0.5 Å of one another) were assigned the same numerical identifier. As in the folate complex, corrections for the X-ray scattering of amorphous solvent (final values uk = 0.75 and ub = 240) and overall thermal anisotropy were used throughout refinement.

After 90 cycles of least-squares refinement the process had converged to a crystallographic R factor of 0.194 for all data measured to 2.3-Å resolution. The rms deviation of bond lengths from their dictionary values was 0.021 Å, and the rms deviation of atoms from their least-squares plane was 0.015 Å for those atoms restrained to lie in a plane (see above). These statistics correspond to a mean uncertainty in atomic position of 0.25 Å as estimated by the method of Luzzati (1952). The final structure (two rhDHFR molecules, 182 residues each) consists of 2948 protein atoms, two 5-deazafolate molecules (64 atoms), and 111 ordered solvent molecules. As in the folate structure, residues 1–3 and 186 in both enzyme molecules, and the 40%-retained amino-terminal initiator methionine (Prendergast et al., 1988), were not modeled because of absent or ambiguous electron density. In addition, the side-chain atoms of E278 beyond C_β were not modeled for similar reasons.

Table I: Recombinant Human DHFR. Secondary Structure

helices		β strands		tight turns[a]	
Pro(II)[b]	21–26	β A	4–10	I	11–14
α B	27–40	β B	47–53	I′	18–21
α C	53–59	β C	71–76	II	43–46
α E	92–102	β D	88–90	I	61–64
α E′	102–109	β E	108–116	II	67–70
α F	117–127	β F	130–139	II	83–86
		β G1[c]	157–159	II	162–165
		β G2[c]	168–172	I′	172–175
		β H	175–185		

[a] Tight turns are classified after the nomenclature of Richardson (1981). [b] Polyproline-like helix (type II, left handed). [c] Strand G, which is continuous in the bacterial DHFR's, is interrupted by a tight turn in the vertebrate enzymes; these discontinuous segments are denoted G1 and G2.

RESULTS

Structure of the rhDHFR·Folate Binary Complex

General Features. Of the two molecules in the asymmetric unit (also the unit cell in space group $P1$) molecule 2 is the more ordered as judged by the quality of the electron density maps and the refined atomic temperature factors. Therefore the results presented here will focus on molecule 2; the structure of molecule 1 will be discussed only when there are significant differences between the two. For clarity we will refer to sequence numbers 1–186 in either molecule.

The folding of rhDHFR, as displayed in Figure 2, is very similar to that previously described for clDHFR (Volz et al., 1982). However, subsequent refinement of the clDHFR·NADPH structure against higher resolution data (1.7 Å, S. J. Oatley, unpublished results) requires that minor corrections be made to those earlier secondary structure assignments. Table I lists the elements of secondary structure present in rhDHFR; they are identical with those found in the higher resolution clDHFR structure. An eight-stranded β sheet consisting of seven parallel strands and a carboxy-terminal antiparallel strand composes the core of the protein. Within strand βG, residues 160–167 form a seven-residue disruption of the β-sheet hydrogen bonding. As a result, βG is not continuous but consists of two consecutive strands denoted G1, residues 157–159, and G2, residues 168–172. This extended beta bulge, termed a "beta blow-out", was first noted in clDHFR (Volz et al., 1982). We further observe that residues

FIGURE 2: α-Carbon representation of human dihydrofolate reductase complexed with folate (molecule 2). β strands are labeled with upper case letters and α helices with lower case.

162–165 of this disruption are in a tight-turn conformation.

Five α helices are packed against the β-sheet core. The helix αB, residues 27–40, is slightly unwound at its carboxy terminus, probably due to the presence of three consecutive threonine residues, which terminate the helix. The conformation in this region is such that the backbone carbonyl oxygen of F34 forms two hydrogen bonds to T38 one turn further along the helix: one with the backbone amide nitrogen and another with the side-chain hydroxyl. This hydrogen-bonding pattern also occurs between Q35 and T39 and between R36 and T40. Of these, T38 is a structurally conserved residue whose suggested role is terminating helix αB and maintaining the orientation, via hydrogen bonding, of the side chain of another structurally conserved residue, R70 (Kraut & Matthews, 1987).

The two-turn helix αE′, which is not present in either lcDHFR or ecDHFR, immediately follows αE, so that the last residue of αE is also the first residue of αE′. The helix αE begins with S92 and ends with the backbone nitrogen of Q102. The helix αE′ begins with the backbone carbonyl oxygen of Q102 and ends at V109. Despite their sharing a common residue (Q102), αE and αE′ are distinct helices, as their axes are nearly perpendicular. This backbone kink may be due to P103, as proline residues are well-documented helix terminators. The helix αE′ arises in part from a four to six residue insertion in vertebrate DHFR relative to the bacterial enzymes.

In addition to the five α helices in the structure, residues 21–26, sequence DLPWPP, form two turns of a polyproline-like helix (left handed, type II). This feature, first noted in clDHFR (Volz et al., 1982), contains residues that interact with folate in this structure and with NADPH in clDHFR. Its absence in ecDHFR and lcDHFR is probably due to insertion in vertebrate DHFR's of a proline residue, P25, immediately before a nonconserved P26 (ec N23, lc H22).

Eight tight turns have been identified in rhDHFR on the basis of backbone torsion angles and hydrogen-bonding patterns and are classified in Table I according to the nomenclature of Richardson (1981). Two cis-peptide linkages are also observed, one between residues R65 and P66 and another between conserved residues G116 and G117, which is near the nicotinamide binding site. The former cis-peptide linkage is present in both lcDHFR (Bolin et al., 1982) and clDHFR (Volz et al., 1982) but not in ecDHFR (Bolin et al., 1982); the latter is a conserved structural feature of all chromosomally encoded DHFR's.

Comparison of the Two Molecules in the Unit Cell. A noncrystallographic approximate 2-fold rotation axis (179°) relating molecules 1 and 2 runs almost parallel to βD at one edge of the β sheet. At the dimer interface the side chains of residues F88, L99, and L105 in molecule 2 and the equivalent residues in molecule 1 form a hydrophobic cluster. Additional stabilization is provided by six intermolecular hydrogen bonds: a hydrogen bond between the backbone amide nitrogen of E104 in molecule 1 and the backbone carbonyl oxygen of H87 in molecule 2; a pair of hydrogen bonds between the side-chain carboxamide of Q102 in molecule 1 and the backbone nitrogen and carbonyl oxygen L89 in molecule 2; and similar hydrogen bonds between E104 of molecule 2 and H87 in molecule 1 and between Q102 of molecule 2 and L89 in molecule 1.

Although the two molecules in the unit cell are in different packing environments, their refined coordinates are quite similar; least-squares superposition with the program OVRLAP (Rossmann & Argos, 1975) yields an rms deviation of 0.4 Å for all 182 α-carbons. The largest deviations in position, greater than 0.9 Å, occur for residues 42–45 (2.6 Å for 44), which make up a loop connecting αB and βB. Residues 43–46 form a type II tight turn, and the side chain of E44 is involved in a crystal contact in molecule 2, but not in molecule 1. As the backbone atoms of E44 have the highest average temperature factor in either molecule 1 or 2, this region appears particularly flexible.

The Folate Binding Site. As was mentioned under Methods, upon completion of the rhDHFR·folate structure refinement there remained unmodeled $F_o - F_c$ difference density near the bound folate. Although this residual density is most prominent in molecule 1, a smaller peak in molecule 2 occupies a position similar to a portion of the larger peak in molecule 1. This extra density in molecule 1 is depicted in Figure 3, along with the folate ligand and several adjacent residues. The density extends from the vicinity of folate's N5, parallel to the pABA moiety, toward the surrounding solvent. Due to obstruction by this extra density in molecule 1, the side chain of F31 is positioned differently in molecules 1 and 2. Of the compounds known to be present in the crystallization medium, only folate is of roughly similar size; however, a folate molecule cannot be convincingly fitted to the extra density. HPLC chromatography of a sample of the folic acid used in the crystallization (Sigma Chemical) yielded a single peak (chromatograph not shown), suggesting that, if impurities are present, their con-

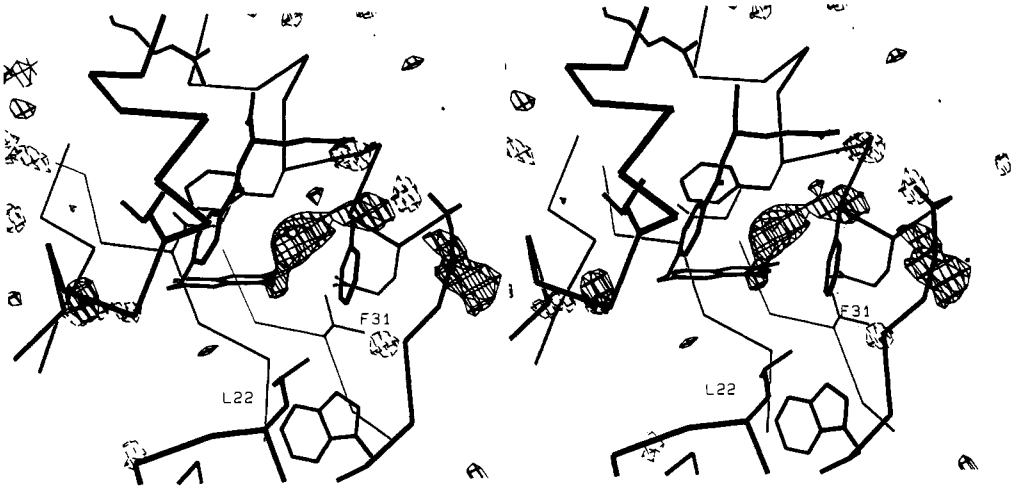

FIGURE 3: Postrefinement ($F_o - F_c$) difference density adjacent to the folate binding site of molecule one. The contour level is $\pm 3.5\sigma$, with negative electron density depicted by dashed lines.

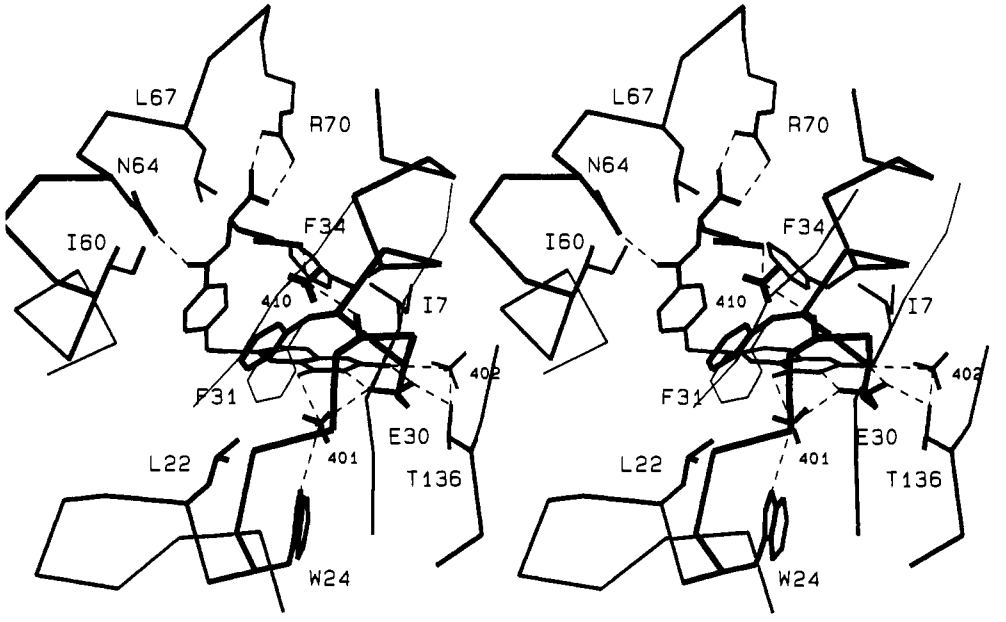

FIGURE 4: Interactions between human dihydrofolate reductase and folate (molecule 2), with hydrogen bonds depicted as dashed lines. Water molecules are displayed as tetrahedra. For comparison, the orientation of F31 in molecule 1 is indicated by thin lines.

centrations are quite low. However, it is possible that this extra density represents a poorly ordered second binding site for folate or that folate oxidation or degradation occurred during crystallization or X-ray data collection, with the extra density representing bound product or products of the process.

The polarity of the substrate binding site, which is formed exclusively of regular secondary structure, is complementary to that of folate. The folate molecule consists of polar pteridine and glutamate moieties linked by a relatively nonpolar benzoyl ring of the pABA group. The pteridine and glutamate segments are surrounded by backbone carbonyls and polar side chains, while the benzoyl portion is in contact with nonpolar side chains of hydrophobic residues. As viewed in Figure 4, the interior of the folate site is formed by residues in strands βA and βE, while the solvent interface is composed of residues participating in the left-handed polyproline helix, the helix αB, the carboxy terminus of αC, and residues 61–70. Residues 61–70 form two tight turns (61–64 and 67–70), joined by a cis-peptide linkage between residues R65 and P66.

We now describe, in greater detail, interactions between the enzyme and bound substrate. Referring again to Figure 4, the pteridine moiety of folate interacts specifically with the following enzyme residues: the 2-amino group is hydrogen bonded to both OE1 of E30 and water molecule 402, the latter of which is also hydrogen bonded to OG1 of T136; N3 is hydrogen bonded to OE2 of E30, and O4 is hydrogen bonded to water 401, which in turn is hydrogen bonded to OE2 of E30 and weakly to the indole nitrogen of W24. No specific interactions occur between the enzyme and N1, N5, N8, or N10 of folate.

The pABA moiety of folate interacts nonspecifically with the side chains of five hydrophobic residues. van der Waals contacts exist between the pABA benzoyl ring and the side chains of F31 (in molecule 2 but not molecule 1; see beginning of this section), F34, I60, P61, and L67. Of these, F34 and L67 are conserved, 61 is either proline or glycine, and 60 is nonpolar in reported sequences. Two interactions exist between the enzyme and the peptide bond joining the pABA and glutamate of folate: a hydrophobic contact with the side chain of L67 and a hydrogen bond between the carbonyl oxygen of pABA and the side-chain amide nitrogen of N64.

The glutamate of folate interacts strongly with a single residue: its α-carboxylate forms two charge-mediated hydrogen bonds with the side-chain guanidinium of the conserved R70. In contrast, the γ-carboxylate does not interact with any residues in molecule 1, while in molecule 2 it is hydrogen

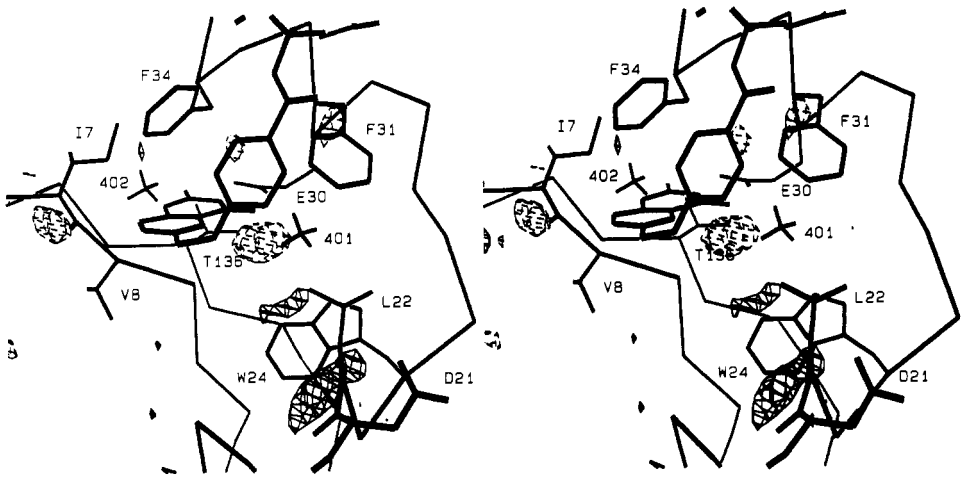

FIGURE 5: Catalytic site of the rhDHFR·folate complex and the 5-deazafolate minus folate difference map contoured at $\pm 4\sigma$. Negative contours are depicted by dashed lines. The view is rotated approximately 90° from that of Figure 4.

bonded to water 410, which in turn forms a hydrogen bond to the backbone carbonyl oxygen of R28. The location of the γ-carboxylate at the bulk–solvent interface, the difference in its interactions with molecules 1 and 2, and the fact that this group possesses the largest temperature factors in the bound folate molecule all suggest that the γ-carboxylate of folate is weakly bound. This is consistent with the observation that pentaglutamyl folate (polymerized via the γ-carboxylate) is a competent substrate for human DHFR (Domin et al., 1982), as the additional glutamate residues could readily extend into the surrounding solvent.

Structure of the rhDHFR·5-Deazafolate Binary Complex

Difference Fourier Analysis. Since crystals of the rhDHFR·5-deazafolate complex are isomorphous with those obtained with folate as the ligand, difference Fourier analysis is a sensitive means of detecting changes between the two structures. Difference electron density maps were calculated with coefficients F_o(5-deazafolate) − F_o(folate), using phases computed from the final refinement cycle of the folate complex. The resultant difference density is not identical for molecules 1 and 2.

The difference density at the catalytic site of molecule 1 is dominated by a negative peak that is coincident with the residual unmodeled positive density in the folate complex (see above). Also, a small negative peak at the catalytic site of molecule 2 is coincident with the residual density in molecule 2 of the folate complex. This observation indicates that the presence of the unidentified ligand in the rhDHFR·folate complex is related to the presence of folate in the crystallization medium and that no such moiety is bound in the rhDHFR·5-deazafolate complex. Two additional difference density peaks in the catalytic site of molecule 1 are not seen in molecule 2. Positive and negative density associated with F31 suggests that this side chain has reoriented, but the proximity of this difference density to the large negative peak mentioned above precluded a more detailed analysis of the movement at this point. The remaining difference density unique to molecule 1 is near the carbonyl oxygen of the pABA group. Its location suggests that the side-chain amide of N64 has moved, relative to its positions in the folate structure.

Three difference density peaks are in similar positions in molecules 1 and 2. Figure 5 is a superposition of the refined coordinates of the rhDHFR·folate complex (molecule 2) and the initial difference map. A negative peak near I7, within strand βA of the β sheet, suggests that in the rhDHFR·5-deazafolate complex the backbone carbonyl oxygen of I7 is closer to the inhibitor's N8 than it was to N8 of folate. Positive density between the inhibitor and residues G20, D21, and L22 suggests that these residues have moved toward the bound 5-deazafolate, as compared to their positions in the folate complex. Finally, positive density adjacent to the side chain of L22 indicates a reorientation, from its position near W24 in the folate complex, to a position in van der Waals contact with C5 of 5-deazafolate in the inhibitor complex.

Comparison of the Refined Structures of the rhDHFR·5-Deazafolate and rhDHFR·Folate Complexes. Direct comparison of refined coordinates for the two complexes indicates changes that are consistent with the difference map. Least-squares superposition of the rhDHFR·folate and rhDHFR·5-deazafolate complexes (molecule 2) results in an rms deviation of 0.3 Å for 182 α-carbons, with the largest positional differences occurring in two discrete regions. In a loop connecting βC and βD, remote from the catalytic site, a difference of 0.7 Å is seen for E78. The temperature factors in this solvent-exposed loop are relatively high in both complexes and, in the 5-deazafolate complex, the side chain of E78 in molecule 2 is disordered, suggestive of multiple conformations for this residue. The second region of protein conformational rearrangement in the 5-deazafolate complex, as compared with the folate complex, is near the ligand's 5-position; the observed movements are consistent with a decrease in polarity at the 5-position consequent on replacement of the pteridine ring's N5 with a carbon. Differences in α-carbon positions of residues 18–21 are greater than 0.4 Å, the largest being 0.8 Å for D20; the direction of movement of these residues is toward C5 of 5-deazafolate. In addition the side chain of L22 reorients, from a position in contact with W24 in the folate complex to a position in contact with C5 of the inhibitor. Also, the side chain of F31, which is in van der Waals contact with the side chain of L22 in the folate complex, has moved slightly while maintaining a van der Waals interaction with the side chain of L22.

Consistent with the expected higher basicity of N8 in 5-deazafolate than in folate [e.g., pyrazine pK_a 0.6 and pyridine pK_a 5.2 (Weast, 1968)], the inhibitor appears to be protonated at N8 in the rhDHFR binary complex whereas folate is not. Inspection of the refined rhDHFR·5-deazafolate structure provides experimental evidence for N8 protonation of 5-deazafolate in the binary complex. The catalytic site of the rhDHFR·5-deazafolate structure is shown in Figure 6. Clearly the binding geometry of 5-deazafolate is similar to that of folate, but a new hydrogen bond between N8 of the inhibitor and the carbonyl oxygen of I7 is formed by rotation of the

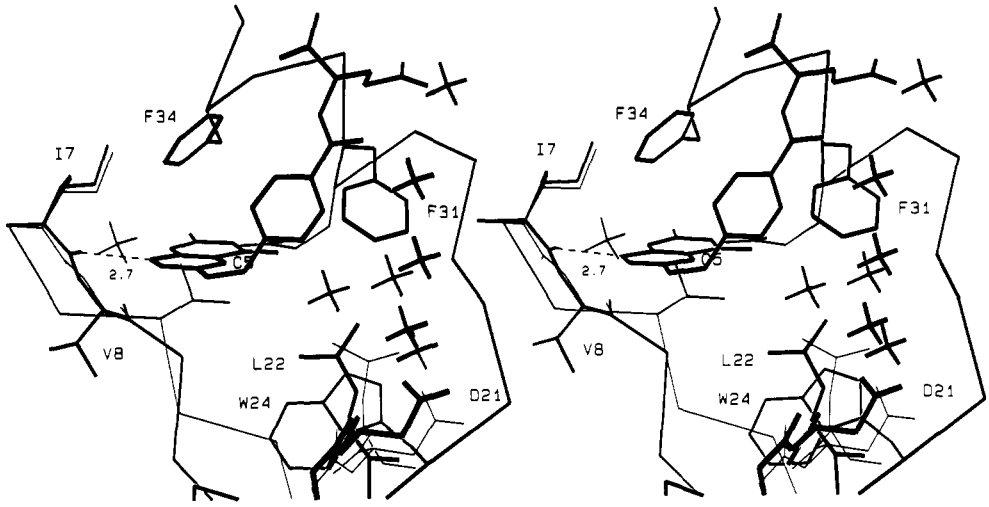

FIGURE 6: Catalytic site of rhDHFR·5-deazafolate complex. Several key residues of the folate complex are indicated by thin lines. The different orientations of D21, L22, and the I7–V8 peptide plane in the two complexes are clearly evident. The hydrogen bond between the inhibitor's N8 and the carbonyl oxygen of I7 is depicted as a dashed line.

I7–V8 peptide plane. This rotation is evidenced by backbone torsion angle differences between the folate and 5-deazafolate complexes. Changes in the ϕ and Ψ angles for I7 are 0° and −21° (−1° and −28° for molecule 1), and 18° and 8° (23° and 6° for molecule 1) for V8. The net result is an ~22° rotation of the I7–V8 peptide plane, positioning the carbonyl oxygen of I7 2.7 Å from N8 of the inhibitor, decreased from 3.3 Å in the folate complex (3.5 Å in molecule 1). This reorientation of the carbonyl oxygen of I7 is consistent with density observed in the initial difference maps (see above).

We have also obtained corroborating evidence, by UV difference spectroscopy, that 5-deazafolate is protonated upon binding to rhDHFR. Changes in the UV spectrum upon binding of 5-deazafolate to rhDHFR strongly resemble the pH 2.0 minus pH 6.5 protonation difference spectrum for the inhibitor in solution (spectra not shown). That a similarity between the pH difference spectrum in solution and the binding difference spectrum indicates proton uptake by a ligand has been demonstrated by calorimetric measurements on methotrexate binding to clDHFR (Subramanian & Kaufman, 1978). In contrast, there is no such evidence for protonation when folate binds to rhDHFR (spectra not shown), clDHFR (Subramanian & Kaufman, 1978), ecDHFR (Poe et al., 1974), lcDHFR (Hood & Roberts, 1978), or bacteriophage T4 specific DHFR (Erickson & Mathews, 1972). Moreover, a semiempirical calculation of the heats of formation of both N1 and N8 protonated 5-deaza-6-methylpteridine (an analogue of 5-deazafolate lacking the pABG moiety) by the AM1 method (Dewar et al., 1985) revealed that N8 protonation is more favorable by 3.9 kcal mol^{-1} (Terry Jones, personal communication). Although these calculations are performed on gas-phase molecules, the AM1 method has proven reliable in the prediction of relative aqueous basicities of ring nitrogens in related heterocyclic systems (Anguiano et al., 1988; Sanz et al., 1988). Together with the structural evidence presented above, these results strongly point to protonation of 5-deazafolate upon binding to rhDHFR, most likely at N8.

When comparing the folate and 5-deazafolate complexes of rhDHFR, two differences are exclusive to molecule 1. In the folate complex, the unidentified moiety bound at the catalytic site of molecule 1 prevents the F31 side chain from occupying a position similar to that seen in molecule 2. In the absence of that extra moiety in the 5-deazafolate complex, the side chains of F31 in molecules 1 and 2 occupy essentially identical positions. In this orientation, the side-chain phenyl ring of F31 makes van der Waals interactions with the pABA ring and O4 of 5-deazafolate and with the side chain of L22. In spite of this increased similarity of the enzyme conformation in molecules 1 and 2 of the 5-deazafolate complex, however, the 5-deazapteridine ring of the inhibitor is displaced toward the nicotinamide binding site in molecule 1 as compared both to its position in molecule 2 and to the position of the pteridine ring of folate in either molecule 1 or 2. The magnitude of this positional difference between the folate and 5-deazafolate ligands in molecule 1 is 0.7 Å for the pABA groups and 0.4 Å for the pyrazine as compared to the deazapyrazine ring. With this binding geometry, the pABA carbonyl oxygen of 5-deazafolate in molecule 1 is too distant from the side chain of N64 to form the hydrogen bond seen in the folate complex and in molecule 2 of the 5-deazafolate complex. In lieu of forming a hydrogen bond to 5-deazafolate, the side chain of N64 rotates away from the ligand binding site to instead form a hydrogen bond to the backbone carbonyl oxygen of P61. We note that residues 61–64 are in a tight turn conformation.

One additional difference exists between molecules 1 and 2 of the 5-deazafolate complex. In molecule 2, four water molecules are bound in proximity to 5-deazafolate that were not seen in the folate complex. One of these waters is located between L22 and W24, in a site occupied by the side chain of L22 in the folate complex. These four water molecules form a hydrogen-bonded bridge between the pABA carbonyl oxygen of 5-deazafolate, the side chain of D21, and the backbone carbonyl oxygen of W24. Equivalent water molecules are not seen in molecule 1.

A Model for NADPH Binding to rhDHFR

A Hypothetical Model of the rhDHFR·NADPH·Folate Complex. In the absence of an rhDHFR crystal structure containing bound cofactor, we have constructed a hypothetical model of the NADPH·folate complex. The model was generated by an α-carbon least-squares superposition of the 1.7-Å refined clDHFR·NADPH coordinates (S. J. Oatley, unpublished results) and the rhDHFR·folate coordinates (molecule 2). No further adjustments were made to the model, owing to the reasonable fit between the cofactor and rhDHFR obtained in this way. A detailed analysis of differences between the clDHFR and rhDHFR structures is presented in the Discussion section, but we mention here that the high degree of similarity in the NADPH binding sites of the two enzymes is reflected in the rms deviation of 0.4 Å for the α-carbons

of 22 residues that contact the cofactor in the clDHFR·NADPH structure.

Of the 22 residues in contact with the cofactor in the clDHFR·NADPH structure, 18 contribute side-chain atoms to those interactions. Only 2 of those 18 residues are not conserved between rhDHFR and clDHFR, and neither is near the folate binding site. Residues T118 and A119 in clDHFR are sequentially equivalent to S118 and S119 in rhDHFR. In clDHFR, the side-chain hydroxyl of T118 forms a hydrogen bond with the nicotinamide pyrophosphate oxygen via an intervening water molecule and in rhDHFR S118 could form an analogous interaction. The following residue in clDHFR, A119, is in van der Waals contact with the cofactor adenine ring, but the side-chain hydroxyl of S119 in rhDHFR is positioned so that it could instead form a hydrogen bond with N7 of the adenine ring. With the exception of clDHFR, this residue is a serine in all known vertebrate sequences, whereas in the bacterial enzymes it can be R, Q, E, or I.

An additional sequence difference between rhDHFR and clDHFR may affect cofactor binding. In rhDHFR, the γ-carboxylate of E123 can be positioned to interact directly with the cofactor adenine ring N7 and exocyclic N6. In the ecDHFR·$NADP^+$ complex a similar interaction occurs between the adenine ring and Q102 (Bystroff, 1988; Bystroff et al., 1990), which occupies the same position as E123 in rhDHFR. In clDHFR the sequentially equivalent A123 does not contact the cofactor. As stated above, S118 is also in a position to interact with the adenine N7. Determination of which, if either, of these proposed interactions actually occurs between rhDHFR and the adenine N7 must await the structure of a cofactor-containing complex.

In our hypothetical model of the rhDHFR·NADPH·folate complex, all other nonspecific and hydrogen-bonding interactions seen in clDHFR can also be formed, and there are no unfavorable contacts between the cofactor and the enzyme. There is, however, a striking overlap of the cofactor nicotinamide ring and the folate pteridine ring in our model: the pteridine ring protrudes approximately 1 Å into the unoccupied nicotinamide binding pocket of the rhDHFR structure. We are convinced this overlap is not merely the result of uncertainty in the precise manner of superposing the two binary complex structures since, as noted above, the rms deviation between α-carbons of the 22 residues in contact with the cofactor is only 0.4 Å (or 0.6 Å for all 182 common residues). In our hypothetical rhDHFR·NADPH·folate model the nicotinamide C4 atom is positioned almost directly under and 2.4 Å away from C7 of folate, while C6 of folate is separated by only 2.6 Å from C4 of the nicotinamide.

A Hypothetical Model of the rhDHFR·NADPH·5-Deazafolate Complex. We have also constructed a hypothetical model of the rhDHFR·NADPH·5-deazafolate complex by least-squares superposition of the clDHFR·NADPH and rhDHFR·5-deazafolate structures. With the exception of differences in the enzyme structure discussed above, the hypothetical ternary complexes with folate and 5-deazafolate are quite similar. The van der Waals surface of the cofactor's nicotinamide ring partially overlaps that of the 5-deazapteridine ring of 5-deazafolate, as it did that of the pteridine ring of folate, with identical distances between the nicotinamide and the heterocycle rings. Therefore the partial overlap of the nicotinamide and heterocycle binding cavities observed in this hypothetical ternary complex appears unrelated to the protonation state at N8 of the heterocycle. We believe this hypothetical rhDHFR·NADPH·5-deazafolate complex possesses some features that are characteristic of the transition state for folate reduction, an idea that is detailed in the Discussion section.

Discussion

Comparison with a Recently Reported rhDHFR·Folate Crystal Structure. The structure of a folate binary complex of human DHFR was recently reported by Oefner et al. (1988). Their crystallization conditions, pH, and space group differ from those reported here. Precipitation with ammonium sulfate at pH 7.0 yielded crystals of space group $R3$ with one molecule in the asymmetric unit. Unfortunately, a detailed comparison cannot be made as we were unable to obtain coordinates for the $R3$ structure. We can say, however, that the general molecular features described in that publication appear similar to those reported here.

Comparison of rhDHFR·Folate and clDHFR·NADPH. As suggested by the 75% sequence homology (140 identical residues out of 186), the structures of clDHFR and rhDHFR are quite similar. The 46 sequence differences occur with nearly equal frequency in helices, β strands, turns, and loops. The longest stretch of identical sequence, residues 50–68, forms portions of both the folate and NADPH binding sites. After least-squares superposition of clDHFR and rhDHFR (molecule 2), the rms deviation in α-carbon positions is 0.6 Å for 182 residues. Excluded from the comparison were three carboxy-terminal residues in clDHFR that are not present in human, bovine, mouse L1210, or porcine DHFR and residues 1–3 and 186, which are not included in the present model of rhDHFR.

The largest positional deviations between rhDHFR and clDHFR occur in regions involved in lattice interactions in one or the other structure. Differences in atomic position for the α-carbons of residues P103, E104, and L105, within the helix αE′, are 2.2, 2.1, and 1.0 Å, respectively. Residues 102 and 104 participate in intermolecular hydrogen bonding at the dimer interface in rhDHFR, while in clDHFR those residues possess the highest average backbone temperature factors, suggesting that conformational flexibility is responsible for these differences. Positional deviations for the α-carbons of residues P61, E62, K63, and N64 are 1.3, 1.2, 1.9, and 1.4 Å, respectively. In the clDHFR·NADPH structure, the side chains of K63 and N64 participate in a lattice interaction, while in rhDHFR the N64 side-chain amide forms a hydrogen bond to the pABA carbonyl oxygen of folate, implying that residues 61–64 are somewhat flexible and able to adopt a different conformation in response to folate binding. We note that attempts to soak folate into clDHFR·$NADP^+$ crystals, which are isomorphous with crystals of the clDHFR·NADPH complex, leads to their dissolution. This phenomenon is probably related to a conformational rearrangement of residues 61–64. When comparing molecule 1 of rhDHFR to clDHFR, an additional conformational difference exists that is not present in molecule 2; deviations in α-carbon positions of residues 42–46, which form part of a solvent-exposed loop connecting αB and βB, are greater than 1 Å. These deviations are probably also related to conformational flexibility in this portion of the rhDHFR molecule since it possesses high temperature factors in molecule 1, while residue E44 participates in a lattice interaction in molecule 2. As a result this region also displays the largest differences between molecules 1 and 2.

Inhibition of rhDHFR by 5-Deazafolate. Based on the present structures, we believe that the greater affinity of DHFR for 5-deazafolate than for folate, as evidenced by the higher K_i of folate in both ecDHFR and clDHFR (Stone et al., 1984), is the result of two factors: (1) exchange of an

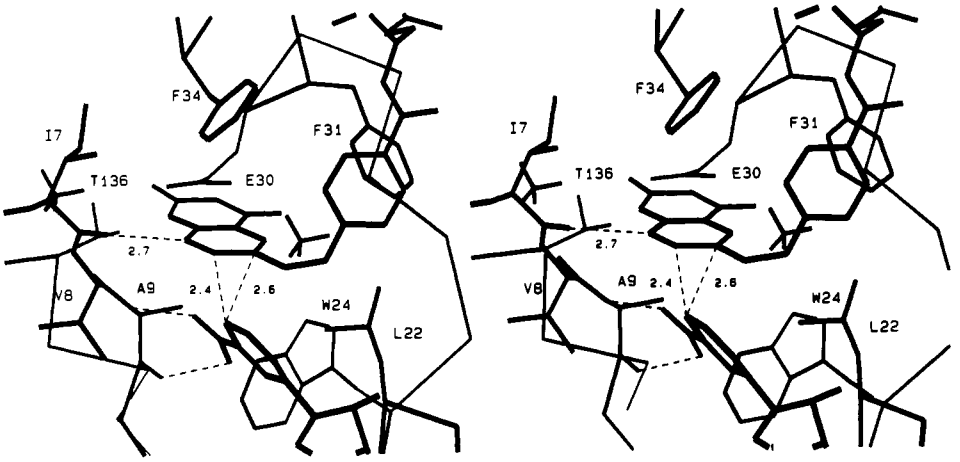

FIGURE 7: Proposed model of the transition state for folate reduction. The coordinates of NADPH were derived from least-squares superposition of the rhDHFR·5-deazafolate and clDHFR·NADPH complexes (see text). Hydrogen bonds are depicted as dashed lines, as are the distances between the hydride donor (nicotinamide C4) and acceptors (substrate C6 and C7).

unfavorable polar–nonpolar interaction between N5 of folate and the side chain of L22 for a favorable nonpolar–nonpolar interaction between C5 of 5-deazafolate and L22; (2) formation of a hydrogen bond between the protonated N8 of 5-deazafolate and the carbonyl oxygen of I7, which is not possible with folate.

Catalysis of Folate Reduction by rhDHFR. The protonation state of the pteridine ring that occurs during folate reduction can be surmised by analogy with 7,8-dihydrofolate reduction. Protonation of dihydrofolate in the transition state, presumably at N5, is indicated by two lines of evidence. In a study of both transient and steady-state kinetics of 7,8-dihydrofolate reduction by rhDHFR, it was concluded that the first enzymic turnover is partially limited by an inferred obligatory isomerization of the ternary substrate complex that is probably associated with proton transfer (Beard et al., 1989). Additionally, based on a study of pH and deuterium isotope effects on the catalysis of 7,8-dihydrofolate reduction by ecDHFR, it was concluded that N5 protonation either immediately precedes or is concerted with hydride transfer (Stone & Morrison, 1988; Morrison & Stone, 1988). In any case 7,8-dihydrofolate would be protonated in the transition state, though it appears to be unprotonated in ground-state binary complexes with clDHFR (Subramanian & Kaufman, 1978), bovine DHFR (Selinsky et al., 1990), ecDHFR (Poe et al., 1974), and bacteriophage T4 specific DHFR (Erickson & Matthews, 1972). By analogy, then, a plausible assumption is that a similar mechanism involving protonation of N8 prior to hydride transfer applies to folate reduction. Preprotonation of N8 has been suggested as a means of promoting hydride transfer to C7 (Huennekens & Scrimgeour, 1964; Gready, 1985), because resonance structures can then be drawn that place a formal positive charge on C7. The resulting partial positive charge on the hydride acceptor should enhance the rate of hydride transfer to that atom. The present structures show that N8 protonation of folate would be promoted by its favorable positioning for formation of a hydrogen bond to the nearby carbonyl oxygen of I7, similar to that observed in the rhDHFR·5-deazafolate structure.

Two geometrical features of the transition state for folate reduction can be surmised from theoretical studies. Ab initio calculation of the transition-state structure for reduction of methyleniminium cation by 1,4-dihydropyridine indicates that a 2.6-Å separation of the donor and acceptor atoms is optimal for hydride transfer (Wu & Houk, 1987). Similar calculations on 1,4-dihydropyridine reduction of cyclopropenium cation point to a transition state in which the nicotinamide ring is nearly planar, with C4 only 0.1 Å out of the plane in the direction of hydride transfer (Donkersloot & Buck, 1981).

As already indicated in the Results section, we believe our hypothetical model of the rhDHFR·NADPH·5-deazafolate complex, generated by least-squares superposition of the clDHFR·NAPDH and rhDHFR·5-deazafolate structures, possesses features suggested above as characteristic of the transition state for folate reduction. Only one superficial change was made to the rhDHFR·NADPH·5-deazafolate model to produce this hypothetical transition-state model for folate reduction: 5-deazafolate's C5 was replaced by N5 of folate. No further adjustments were made to the enzyme molecule or to either ligand. No out-of-plane shifts of pteridine ring atoms of folate or of the nicotinamide ring atoms of NADPH were made since (1) the crystal structure of folic acid contains a planar pteridine (Mastropaolo et al., 1980), (2) the crystal structure of *N*-benzyl-1,4-dihydronicotinamide revealed a planar nicotinamide ring (Karle, 1961), and (3) theoretical studies on the reduction of cyclopropenium cation by 1,4-dihydropyridine indicate an early, reactant-like transition state (Donkersloot & Buck, 1981). This hypothetical transition-state model, depicted in Figure 7, possesses three key characteristics expected of the transition state for folate reduction. First, the pteridine is protonated at N8. Second, a hydrogen bond is formed between the protonated pteridine's N8 and the carbonyl oxygen of I7. And third, the close 2.4-Å approach of the nicotinamide C4 and pteridine C7 atoms (to be compared with an expected van der Waals distance of 3.7 Å in the case of $NADP^+$ or 3.9 Å in the case of NADPH) approximates the 2.6 Å theoretical optimum for hydride transfer noted above.

That the nicotinamide and pteridine binding sites partially overlap was hinted at in both the clDHFR·$NADP^+$·biopterin (Freisheim & Matthews, 1984) and ecDHFR·$NADP^+$·folate structures (Bystroff et al., 1990). The distance between the nicotinamide C4 and pteridine C7 atoms was 3.0 Å in the clDHFR structure and 3.1 Å in the ecDHFR structure, with movement of either ligand to relieve this compression being disfavored by numerous interactions with the enzyme molecule. Though not as dramatically shortened as the 2.4-Å separation between the same atoms in the present hypothetical transition-state model, it is significantly less than the expected 3.5-Å van der Waals contact distance. Figure 8 depicts a superposition of the hypothetical transition-state model presented herein and the ecDHFR·$NADP^+$·folate structure (Bystroff et

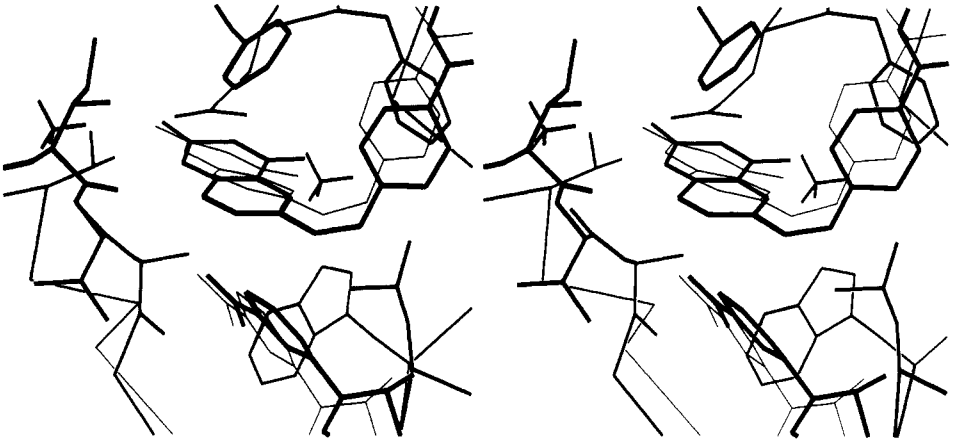

FIGURE 8: Comparison of the hypothetical transition-state model for folate reduction (Figure 7) with the binding geometry of folate and $NADP^+$ (thin lines) in the ternary ecDHFR·$NADP^+$·folate complex.

al., 1990). The difference in pteridine binding geometry between the two is best described as a 20° rotation about an axis approximately colinear with the C4A–N5 bond. It is obvious that, in the ecDHFR structure, steric repulsion with the nicotinamide ring prevents the pteridine from assuming the geometry it has in our hypothetical model—except in the transition state for hydride transfer, where a 2.6-Å separation is expected. In contrast to this implied sensitivity of the pteridine binding geometry to occupancy of the nicotinamide binding site, the nicotinamide binding geometry is essentially identical in the clDHFR·NADPH and clDHFR·$NADP^+$·biopterin structures (Freisheim & Matthews, 1984), suggesting that the nicotinamide binding geometry is unperturbed by the binding of a pteridine ring. Nevertheless, the nicotinamide ring is disordered in the ecDHFR·$NADP^+$ structure (Bystroff et al., 1990) but ordered and bound in the ecDHFR·$NADP^+$·folate complex, which seems to imply that binding of substrate induces ordering of the nicotinamide ring in ecDHFR. However, since the ecDHFR·NADPH and ecDHFR·$NADP^+$·folate complexes crystallize in one space group and the ecDHFR·$NADP^+$ complex in another (Bystroff et al., 1990), it is possible that binding of folate to the ecDHFR·NADPH complex does not affect binding of the reduced cofactor's nicotinamide ring as it does that of the oxidized cofactor.

Implications for 7,8-Dihydrofolate Binding to rhDHFR. In some respects, 5-deazafolate is also a geometrical analogue of 7,8-dihydrofolate. A crystal structure of 6-methyl-7,8-dihydropterin reveals that the pteridine ring and N8 hydrogen are essentially coplanar (Bieri, 1977). If the same is true of 7,8-dihydrofolate, then the bound 5-deazafolate, protonated at N8, should be geometrically similar to 7,8-dihydrofolate. Thus, since folate and 5-deazafolate are observed to occupy essentially identical positions when bound to rhDHFR, we can surmise that any orientational differences between bound folate and 7,8-dihydrofolate are also likely to be minor. However, comparing enzyme conformations in the rhDHFR folate and 5-deazafolate complexes, a small geometrical difference involving a segment of backbone chain is readily apparent, suggesting that the enzyme molecule itself may readjust slightly in response to the bound pteridine's oxidation state. As described above, a hydrogen bond between the protonated N8 of 5-deazafolate and the carbonyl oxygen of I7 is formed not by reorientation of the heterocycle but by a 22° rotation of the I7–V8 peptide plane to bring the carbonyl oxygen of I7 within hydrogen-bonding distance of N8 of 5-deazafolate. Furthermore, comparison of the rhDHFR·5-deazafolate, clDHFR·NADPH, lcDHFR·NADPH·methotrexate, and ecDHFR·$NADP^+$·folate structures reveals that the peptide planes structurally-equivalent to I7–V8 (that is, cl I7–V8, lc L4–W5, ec I5–A6) occupy similar positions relative to the catalytic site and that formation of a hydrogen bond to N8 of a bound substrate is possible after rotation of the equivalent peptide plane in all four species of DHFR. We recently reported a hypothetical model of the ternary ecDHFR·NADPH·7,8-dihydrofolate Michaelis complex in which the hydrogen bond between N8 of 7,8-dihydrofolate and the carbonyl oxygen of I5 (rh I7) was instead formed by a 7° rotation of the pteridine ring relative to its position observed in the ecDHFR·$NADP^+$·folate structure (Bystroff et al., 1990). The rationale behind this method of forming the hydrogen bond was that it simultaneously repositions C6 of the substrate more directly over the hydride donor, nicotinamide C4, and normalizes the hydrogen-bond geometry between the carboxylate oxygens of D27 and both N3 and the 2-amino group of 7,8-dihydrofolate. Alternatively, it is possible to satisfy these three criteria nearly as well by (1) reorienting folate's pteridine ring to a position analogous to that of the heterocycle in the rhDHFR·5-deazafolate complex, (2) rotating the I5–A6 (rh I7–V8) peptide plane so that the carbonyl oxygen of I5 forms a hydrogen bond with N8 of 7,8-dihydrofolate, and (3) adjusting the side-chain torsion angles of D27 (rh E30). It remains to be seen whether the aforementioned peptide plane rotation, allowing formation of a hydrogen bond between the ligand's N8 and the protein, is unique to rhDHFR or is a general feature of DHFR. Regardless of the geometrical adjustments required for its formation, a hydrogen bond between N8 of substrate and the carbonyl oxygen of I7 cannot perform the same function in the reduction of both folate and 7,8-dihydrofolate. Since 7,8-dihydrofolate has a hydrogen atom attached to N8, a hydrogen bond between N8 and the carbonyl oxygen of I7 is likely to form in the ground-state complex, whereas an equivalent hydrogen bond to N8 of folate is formed only in the transition state.

Differences in the Reactivity of Folate and 7,8-Dihydrofolate. With respect to the chemical step in substrate reduction, hydride transfer from NADPH is much more facile to C6 of 7,8-dihydrofolate than to C7 of folate. For ecDHFR, a comparison of steady-state rates of folate reduction at pH 5, utilizing NADPH and its C4-deuterated counterpart, yielded an isotope effect of 5 in both k_{cat} and k_{cat}/K_m, implicating hydride transfer as the rate-limiting step in the reaction (E. E. Howell, personal communication). Thus the value of 0.01 s^{-1} for k_{cat} obtained from steady-state kinetic measurements represents the rate of hydride transfer. When compared to the reported rate of 950 s^{-1} for the reduction of 7,8-dihydrofolate at pH 5 (Fierke et al., 1987), it is clear that ecDHFR

is 10^5 better as a transition-state template for 7,8-dihydrofolate reduction than for folate reduction.

Referring to Figure 7, we suggest that three important differences between the mechanisms of folate and 7,8-dihydrofolate reduction bear on this differential reactivity. First, preprotonation of the substrate ring nitrogens adjacent to the hydride-accepting carbon leads to a transition-state-stabilizing hydrogen bond for folate but to an unfavorable ionic–nonpolar interaction for 7,8-dihydrofolate. However, in the latter case the unfavorable interaction between the protonated N5 of 7,8-dihydrofolate and the side chain of L22 favors delocalization of the positive charge to C6. Second, ab initio calculations suggest that gas-phase protonation of folate's N8 results in extensive delocalization of the positive charge to the pyrimidine ring, whereas protonation of 7,8-dihydrofolate's N5 leads instead to a relatively localized positive charge buildup on the adjacent C6 (Gready, 1985). In addition, the N8-to-enzyme hydrogen bond, suggested to stabilize the transition state for folate reduction, offers a path for further positive charge delocalization of N8-protonated folate, thereby depleting the already small partial positive charge on C7. This suggests that hydride transfer should be more rapid in the reduction of 7,8-dihydrofolate than of folate as positive charge on the hydride acceptor is thought to promote hydride transfer (Huennekens & Scrimgeour, 1964; Gready, 1985). A third difference concerns the relative orientations of the hydride donor and acceptor atoms for hydride transfer to C7 of folate on the one hand and to C6 of 7,8-dihydrofolate on the other. Theoretical calculations on the reduction of methyleniminium cation by 1,4-dihydropyridine found that the syn transition state is 1.4 kcal mol^{-1} more stable than anti (Wu & Houk, 1987). While the substrate C–N double bonds that are reduced are not strictly syn or anti, the C6–N5 bond is closer to syn, while the C7–N8 bond is more nearly anti. Also, the angle defined by the donor–hydride–acceptor atoms is 154° for hydride transfer to C6 of 7,8-dihydrofolate as measured in the hypothetical transition state model described above, which is considerably closer to the optimal value of 158° for syn hydride transfers observed in theoretical studies (Wu & Houk, 1987) than the 209° angle for hydride transfer to C7 of folate (measured in the same hypothetical complex) is to the 173° optimum value for anti hydride transfer transition states (Wu & Houk, 1987).

Although there must be basic differences in the mechanisms of folate and 7,8-dihydrofolate reduction, a common geometrical feature of both hypothetical transition states is the partial overlap of the pteridine and nicotinamide binding sites. More than simply juxtaposing the reactants, this partial overlap of the ligand binding sites favors binding of the reactive atoms at the distance thought to be optimal for hydride transfer.

We recently reported a hypothetical model of the ecDHFR transition state for 7,8-dihydrofolate reduction, based on the ternary ecDHFR·$NADP^+$·folate complex (Bystroff et al., 1990). It differs from the current model of the transition state for folate reduction in rhDHFR in two respects. First, there is a difference in the binding geometry of the pteridine rings that is best described as a 20° rotation about an axis approximately colinear with the C4A-N5 bond and an additional 7° rotation about an axis perpendicular to the plane of the pteridine ring. Second, in the ecDHFR model, both C6 and C7 of 7,8-dihydrofolate were shifted 0.5 Å out of the pteridine plane in opposite directions, resulting in a 2.6-Å separation of nicotinamide's C4 and 7,8-dihydrofolate's C6. No such movement of pteridine ring atoms was made in the transition-state model for folate reduction by rhDHFR, since the hydride donor and acceptor atoms were already quite close (2.4 Å) after least-squares superposition of the two binary complexes: clDHFR·NADPH and rhDHFR·5-deazafolate (see above). The key factor that led to different pteridine binding geometries in the two models was the manner in which a hydrogen bond was formed between substrate's N8 and the backbone carbonyl oxygen (rh I7, ec I5): either by rearrangement of the backbone chain in the case of folate reduction by rhDHFR or by reorientation of the pteridine ring in the case of 7,8-dihydrofolate reduction by ecDHFR. Although somewhat different in detail, both models exhibit a separation between the reacting atoms that is close to the theoretical 2.6-Å transition-state optimum.

Location of the Catalytic-Site Acid Group. That the conserved acidic side chain at the catalytic site (E30 in rhDHFR; D27 in ecDHFR) does not directly interact with N8 of folate or with N5 of 7,8-dihydrofolate, the presumed proton acceptors, seemed at first perplexing. However enzyme conformational changes in response to replacement of N5 of folate by C5 of 5-deazafolate suggest an explanation. Specifically, the rearrangement of residues 18–22, in particular movement of the L22 side chain to a position in van der Waals contact with 5-deazafolate's C5, suggests that, as would be expected, the side chain prefers association with the more hydrophobic C5 rather than with N5. Moreover, if N5 is protonated in the transition state for 7,8-dihydrofolate reduction, the resulting ionic–nonpolar interaction would be even more unfavorable. However, juxtaposition of a protonated N5 and L22 should encourage delocalization of the positive charge from N5 to C6 and thereby favor the proposed transition state for hydride transfer. In contrast, direct interaction between the side-chain carboxylate of E30 in rhDHFR or D27 in ecDHFR and either N5 or N8 of substrate might instead result in a stable charge-mediated hydrogen bond, thus interfering with charge delocalization to the adjacent carbon atom. Just such a strong hydrogen bond is seen in complexes of the tight-binding inhibitor methotrexate with clDHFR (Subramanian & Kaufman, 1978), bovine DHFR (Cocco et al., 1983), ecDHFR (Schlegel et al., 1981; Bolin et al., 1982), and lcDHFR (Hood & Roberts, 1978; Cocco et al., 1981; Bolin et al., 1982). To study the role of the carboxylic acid group, a site-directed mutant of ecDHFR was constructed, replacing D27 with asparagine (D27N) (Howell et al., 1986). As judged by UV difference binding spectroscopy, methotrexate appeared to bind to the D27N mutant in the unprotonated state (Howell et al., 1986), confirmation of which was obtained by monitoring the binding of ^{13}C-enriched methotrexate to the mutant enzyme (London et al., 1986). As compared to the native enzyme, the decrease in binding energy of methotrexate to the D27N mutant was calculated as 3.9 kcal mol^{-1} for the binary complex and 5.2 kcal mol^{-1} for the NADPH-containing ternary complex (Appleman et al., 1988a). These findings underscore the need to avoid direct interaction between the catalytic carboxylic group and the proton acceptor to circumvent formation of an overly stable protonated intermediate.

Although pathways for indirect protonation of 7,8-dihydrofolate at N5 by the conserved catalytic-site acid group have been proposed (Taira et al., 1987; Morrison & Stone, 1988; Bystroff et al., 1990), a similar mechanism for N8 protonation of folate does not appear feasible. Referring to Figure 4, protonation of folate's N8 via a similar pathway would involve proton shuttling from E30 via water 402 and the 2-amino and N1 groups of folate. In the rhDHFR·folate structure, water 402 is hydrogen bonded to E30, T136, and the 2-amino group of folate, but is 4.6 Å from N1, direct

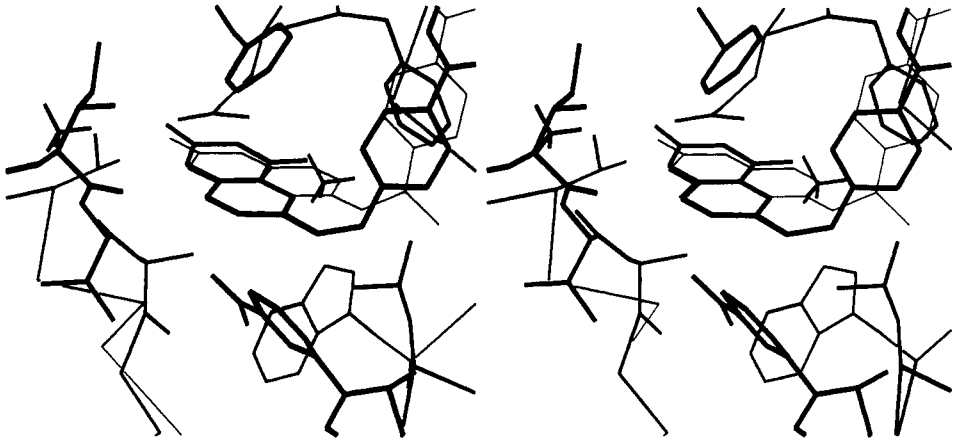

FIGURE 9: Comparison of the hypothetical transition state for folate reduction (Figure 7) and the binding geometry of methotrexate (thin lines) in the ecDHFR·methotrexate structure.

interaction being prevented by the side chain of I7 above and by backbone atoms of βA below. Reorientation of I7 to allow access of water 402 to substrate N1 by rotation of the side-chain C_α–C_β bond is blocked by the indole side chain of W113. Even if folate's N1 were protonated by this means, there is no structurally obvious mechanism for transferring the proton from N1 of folate to N8. Nevertheless slow protonation of N8 may not explain the lower rate of reduction of folate than of 7,8-dihydrofolate, at least in the case of *E. coli* DHFR, since, as mentioned above, hydride transfer to folate is rate limiting (E. E. Howell, personal communication).

Methotrexate Binding to DHFR. Comparison of the ecDHFR·methotrexate and lcDHFR·NADPH·methotrexate structures (Bolin et al., 1982; Filman et al., 1982) suggests that the presence of cofactor does not alter the orientation of methotrexate relative to the enzyme. This observation stands in direct contrast to distortion of the folate binding geometry in the presence of the nicotinamide ring of the cofactor, seen in the ternary ecDHFR·$NADP^+$·folate complex and suggested above as due to partial overlap of the cofactor and substrate binding sites. In Figure 9 we show a superposition of two structures: ecDHFR·methotrexate (Bolin et al., 1982; Filman et al.,1982) and our hypothetical ternary transition state model of rhDHFR. The pteridine rings of folate and methotrexate are essentially coplanar. However, due to the "inverted" binding geometry of methotrexate's pteridine ring, no methotrexate atoms occupy positions geometrically equivalent to those occupied by C6 and C7 of folate in the binary rhDHFR·folate complex, the pteridine ring atoms that partially overlap the nicotinamide C4 position. We believe that the greater stability of ternary DHFR·NADPH·methotrexate complexes as compared with ternary substrate or product complexes (Stone & Morrison, 1986; Fierke et al., 1987; Appleman et al., 1988b, 1990) is at least partly due to the ability of methotrexate and NADPH to bind simultaneously to DHFR without a steric clash occurring between them.

CONCLUSIONS

On the basis of the structures presented herein, different stereochemical mechanisms are proposed for DHFR-catalyzed reduction of folate and 7,8-dihydrofolate by NADPH. However, evidence was found suggesting a common feature of both transition states: a 1-Å overlap of the binding sites of folate's pteridine ring and the nicotinamide ring of NADPH. Despite a similar overlap, tighter binding of 5-deazafolate to DHFR appears to be due in part to formation at N8 of an additional ligand–enzyme hydrogen bond beyond those formed in the folate complex. No such overlap occurs when methotrexate occupies the substrate site, possibly contributing to that inhibitor's extremely tight binding to DHFR.

ACKNOWLEDGMENTS

We thank David Matthews for preliminary experiments and suggesting the crystallization conditions that proved successful, Steven Edwards for assistance with data collection, Christopher Bystroff and Jimin Wang for advice on molecular replacement and other computations, Axel Brünger for installation of his X-PLOR package of crystallographic refinement programs, and both J. Matthew Mauro and Mark Miller for editorial revisions. We also acknowledge a generous grant of computer time from the San Diego Supercomputer Center.

REFERENCES

Anguiano, J., & Sanz, J. F. (1988) *J. Org. Chem. 53*, 3900–3903.

Appleman, J. R., Howell, E. E., Kraut, J., Kühl, M., & Blakley, R. L. (1988a) *J. Biol. Chem. 263*, 9187–9198.

Appleman, J. R., Prendergast, N., Delcamp, T. J., Freisheim, J. H., & Blakley, R. L. (1988b) *J. Biol. Chem. 263*, 10304–10313.

Appleman, J. R., Beard, W. A., Delcamp, T. J., Prendergast, N. J., Freisheim, J. H., & Blakley, R. L. (1990) *J. Biol. Chem. 265*, 2740–2748.

Beard, W. A., Appleman, J. R., Delcamp, T. J., Freisheim, J. H., & Blakley, R. L. (1989) *J. Biol. Chem. 264*, 9391–9399.

Bieri, J. H. (1977) *Helv. Chim. Acta 60*, 2303–2308.

Blakley, R. L. (1969) in *Frontiers of Biology, Vol. 13, The Biochemistry of Folic Acid and Related Pteridines* (Neuberger, A., & Tatum, E. L., Eds.) pp 80–81, North-Holland Publishing Co., Amsterdam-London.

Blakley, R. L. (1984) in *Folates and Pterins, Vol. 1, Chemistry and Biochemistry of Folates* (Blakley, R. L., & Benkovic, S. J., Eds.) pp 191–253, John Wiley & Sons, New York.

Bolin, J. T., Filman, D. J., Matthews, D. A., Hamlin, R. C., & Kraut, J. (1982) *J. Biol. Chem. 257*, 13650–13662.

Brünger, A. T. (1988a) *J. Mol. Biol. 203*, 803–816.

Brünger, A. T. (1988b) X-PLOR Manual, Yale University.

Brünger, A. T., Kuriyan, J., & Karplus, M. (1987) *Science 235*, 458–460.

Bystroff, C. (1988) Ph.D. Thesis, University of California, San Diego, La Jolla, CA.

Bystroff, C., Oatley, S. J., & Kraut, J. (1990) *Biochemistry 29*, 3263–3277.

Cocco, L., Temple, C., Jr., Montgomery, J. A., London, R. E., & Blakley, R. L. (1981) *Biochem. Biophys. Res. Commun. 100*, 413–419.

Cocco, L., Roth, B., Temple, C., Jr., Montgomery, J. A., London, R. E., & Blakley, R. L. (1983) *Arch. Biochem. Biophys. 226*, 567–577.
Cork, C., Fehr, D., Hamlin, R., Vernon, W., Xuong, N.-h., & Perez-Mendez, V. (1973) *J. Appl. Crystallogr. 7*, 319–323.
Crowther, R. A. (1972) in *The Molecular Replacement Method* (Rossmann, M. G., Ed.) pp 173–178, Gordon and Breach, New York.
Dempsey, S. (1987) *Molecular Modeling System (MMS)*, Department of Chemistry Computer Facility, University of California, San Diego, La Jolla, CA.
Dewar, M. J. S., Zoebisch, E. G., Healy, E. F., & Stewart, J. P. (1985) *J. Am. Chem. Soc. 107*, 3902–3909.
Domin, B. A., Cheng, Y.-c., & Hakala, M. T. (1982) *Mol. Pharmacol. 21*, 231–238.
Donkersloot, M. C. A., & Buck, H. M. (1981) *J. Am. Chem. Soc. 103*, 6549–6554.
Erickson, J. S., & Mathews, C. K. (1972) *J. Biol. Chem. 247*, 5661–5667.
Fierke, C. A., Johnson, K. A., & Benkovic, S. J. (1987) *Biochemistry 26*, 4085–4092.
Filman, D. J., Bolin, J. T., Matthews, D. A., & Kraut, J. (1982) *J. Biol. Chem. 257*, 13663–13672.
Freisheim, J. H., & Matthews, D. A. (1984) in *Folate Antagonists as Therapeutic Agents* (Sirotnak, F. M., Burchall, J. J., Ensminger, W. D., & Montgomery, J. A., Eds.) Vol. 1, pp 69–131, Academic Press, Inc., Orlando.
Gready, J. E. (1985) *Biochemistry 24*, 4761–4766.
Hendrickson, W. A. (1981) in *Refinement of Protein Structures* (Machin, P. A., Campbell, J. W., & Elder, M., Eds.) pp 1–8, Daresbury Laboratory, Warrington.
Hood, K., & Roberts, G. C. K. (1978) *Biochem. J. 171*, 357–366.
Howell, E. E., Villafranca, J. E., Warren, M. S., Oatley, S. J., & Kraut, J. (1986) *Science 231*, 1123–1128.
Huennekens, F. M., & Scrimgeour, K. G. (1964) in *Pteridine Chemistry* (Pfleiderer, W., & Taylor, E. C., Eds.) pp 355–376, Pergamon, Oxford.
Jones, T. A. (1978) *J. Appl. Crystallogr. 11*, 268–272.
Karle, I. L. (1961) *Acta Crystallogr. 14*, 497–502.
Konnert, J. H. (1976) *Acta Crystallogr. A32*, 614–617.
Kraut, J., & Matthews, D. A. (1987) in *Biological Macromolecules and Assemblies* (Jurnak, F. A., & McPherson, A., Eds.) Vol. 3, pp 1–72, John Wiley & Sons, New York.
London, R. E., Howell, E. E., Warren, M. S., Kraut, J., & Blakley, R. L. (1986) *Biochemistry 25*, 7229–7235.
Luzzati, V. (1952) *Acta Crystallogr. 5*, 802–810.
Mastropaolo, D., Camerman, A., & Camerman, N. (1980) *Science 210*, 334–336.
Matthews, D. A., Bolin, J. T., Burridge, J. M., Filman, D. J., Volz, K. W., Kaufman, B. T., Beddell, C. R., Champness, J. N., Stammers, D. K., & Kraut, J. (1985a) *J. Biol. Chem. 260*, 381–391.
Matthews, D. A., Bolin, J. T., Burridge, J. M., Filman, D. J., Volz, K. W., & Kraut, J. (1985b) *J. Biol. Chem. 260*, 392–399.
Matthews, D. A., Smith, S. L., Baccanari, D. P., Burchall, J. J., Oatley, S. J., & Kraut, J. (1986) in *Chemistry and Biology of Pteridines 1986* (Cooper, B. A., & Whitehead, V. M., Eds.) pp 789–797, Walter de Gruyter & Co., Berlin.
Morrison, J. F., & Stone, S. R. (1988) *Biochemistry 27*, 5499–5506.
Oefner, C., D'arcy, A., & Winkler, F. K. (1988) *Eur. J. Biochem. 174*, 377–385.
Poe, M., Greenfield, N. J., Hirshfield, J. M., & Hoogsteen, K. (1974) *Cancer Biochem. Biophys. 1*, 7–11.
Prendergast, N. J., Delcamp, T. J., Smith, P. L., & Freisheim, J. H. (1988) *Biochemistry 27*, 3664–3671.
Richardson, J. S. (1981) *Adv. Protein Chem. 34*, 167–339.
Rossman, M. G., & Argos, P. (1975) *J. Biol. Chem. 250*, 7525–7532.
Sanz, J. F., Anguiano, J., & Vilarrasa, J. (1988) *J. Comput. Chem. 9*, 784–789.
Schlegel, H. B., Poe, M., & Hoogsteen, K. (1981) *J. Mol. Pharmacol. 20*, 154–158.
Selinsky, B. S., Perlman, M. E., London, R. E., Unkefer, C. J., Mitchell, J., & Blakley, R. L. (1990) *Biochemistry 29*, 1290–1296.
Stammers, D. K., Champness, J. N., Beddell, C. R., Dann, J. G., Eliopoulos, E., Geddes, A. J., Ogg, D., & North, A. C. T. (1987) *FEBS Lett. 218*, 178–184.
Stone, S. R., & Morrison, J. F. (1986) *Biochim. Biophys. Acta 869*, 275–285.
Stone, S. R., & Morrison, J. F. (1988) *Biochemistry 27*, 5493–5499.
Stone, S. R., Montgomery, J. A., & Morrison, J. F. (1984) *Biochem. Pharmacol. 33*, 175–179.
Subramanian, S., & Kaufman, B. T. (1978) *Proc. Natl. Acad. Sci. U.S.A. 75*, 3201–3205.
Sussman, J. L., Holbrook, S. R., Church, G. M., & Kim, S.-H. (1977) *Acta Crystallogr. A33*, 800–804.
Taira, K., Chen, J.-T., Fierke, C. A., & Benkovic, S. J. (1987) *Bull. Chem. Soc. Jpn. 60*, 3025–3030.
Tanaka, N. (1977) *Acta Crystallogr. A33*, 191–193.
Temple, C., Jr., Elliott, R. D., & Montgomery, J. A. (1982) *J. Org. Chem. 47*, 761–764.
Volz, K. W., Matthews, D. A., Alden, R. A., Freer, S. T., Hansch, C., Kaufman, B. T., & Kraut, J. (1982) *J. Biol. Chem. 257*, 2528–2536.
Wang, J. (1988) Ph.D. Thesis, University of California, San Diego, La Jolla, CA.
Wang, J., Mauro, J. M., Edwards, S. L., Oatley, S. J., Fishel, L. A., Ashford, V. A., Xuong, N.-h., & Kraut, J. (1990) *Biochemistry 29*, 7160–7173.
Weast, R. C., Ed. (1968) *CRC Handbook of Chemistry and Physics*, 49th ed., p D-88, The Chemical Rubber Co., Cleveland, OH.
Wu, Y.-D., & Houk, K. N. (1987) *J. Am. Chem. Soc. 109*, 2226–2227.
Xuong, N.-h., Nielsen, C. P., Hamlin, R., & Anderson, D. H. (1985) *J. Appl. Crystallogr. 18*, 342–350.